PHYSICAL REVIEW A **77**, 012317 (2008)

Quantum-limited metrology with product states

Sergio Boixo,[1,2] Animesh Datta,[1] Steven T. Flammia,[1,3,*] Anil Shaji,[1] Emilio Bagan,[1,4] and Carlton M. Caves[1,5]

[1]*Department of Physics and Astronomy, MSC07-4220, University of New Mexico, Albuquerque, New Mexico 87131-0001, USA*

[2]*Los Alamos National Laboratory, Los Alamos, New Mexico 87545, USA*

[3]*Perimeter Institute for Theoretical Physics, Waterloo, Ontario, Canada N2L 2Y5*

[4]*Grup de Física Teòrica, Universitat Autònoma de Barcelona, 08193 Bellaterra, Barcelona, Spain*

[5]*Department of Physics, University of Queensland, Brisbane, Queensland 4072, Australia*

(Received 20 October 2007; published 15 January 2008)

We study the performance of initial product states of n-body systems in generalized quantum metrology protocols that involve estimating an unknown coupling constant in a nonlinear k-body ($k \ll n$) Hamiltonian. We obtain the theoretical lower bound on the uncertainty in the estimate of the parameter. For arbitrary initial states, the lower bound scales as $1/n^k$, and for initial product states, it scales as $1/n^{k-1/2}$. We show that the latter scaling can be achieved using simple, separable measurements. We analyze in detail the case of a quadratic Hamiltonian ($k=2$), implementable with Bose-Einstein condensates. We formulate a simple model, based on the evolution of angular-momentum coherent states, which explains the $O(n^{-3/2})$ scaling for $k=2$; the model shows that the entanglement generated by the quadratic Hamiltonian does not play a role in the enhanced sensitivity scaling. We show that phase decoherence does not affect the $O(n^{-3/2})$ sensitivity scaling for initial product states.

DOI: 10.1103/PhysRevA.77.012317 PACS number(s): 03.67.Lx, 03.65.Ta, 06.20.Dk

I. INTRODUCTION

Parameter estimation is a fundamental physical task. It typically involves picking a physical system whose state, through its evolution, depends on the value of the parameter. In most quantum metrology schemes [1–18], this system, which we call the "probe," is a composite made up of n elementary quantum constituents. The influence of the unknown parameter γ on the probe is described by an n-body Hamiltonian

$$H_\gamma = \gamma H, \tag{1.1}$$

in which γ appears as a coupling constant and H is a dimensionless coupling Hamiltonian (we use units with $\hbar=1$, so γ has units of frequency). The precision with which γ can be determined depends on the initial state of the probe, the nature of the parameter-dependent Hamiltonian, and the measurements that are performed on the probe to extract information about the parameter. Other factors, such as decoherence in the probe [3,19–21], also have an effect on the achievable sensitivity.

The appropriate measure of the precision with which γ can be determined is the units-corrected mean-square deviation of the estimate $\gamma_{\rm est}$ from the true value γ [22,23],

$$\delta\gamma = \left\langle \left(\frac{\gamma_{\rm est}}{|d\langle \gamma_{\rm est}\rangle/d\gamma|} - \gamma \right)^2 \right\rangle^{1/2}. \tag{1.2}$$

This estimator uncertainty is inversely proportional to the displacement in Hilbert space of the state of the probe corresponding to small changes in γ. The fundamental limit on the precision of parameter estimation,

$$\delta\gamma \geq \frac{1}{\sqrt{\nu}} \frac{1}{2t\Delta H}, \tag{1.3}$$

called the *quantum Cramér-Rao bound* (QCRB) [22–25], is an expression of the maximum amount the state can change under the evolution due to H_γ. In Eq. (1.3), ν is the number of trials with independent, identical probes, t is the time for which each probe evolves under H_γ, and $\Delta H = (\langle H^2\rangle - \langle H\rangle^2)^{1/2}$ denotes the uncertainty in H for each probe, which does not change under the evolution due to H_γ. The QCRB is independent of the choice of estimator and is achievable asymptotically in the limit of a large number of trials, provided the initial state of the probe is a pure state. If the initial state of the probe is not pure or if nonunitary processes destroy the purity of the initial state, the bound (1.3) is not tight, and a stricter version of the QCRB, given in [22–25], can be used, but we have no need for this stricter bound in this paper.

The uncertainty in H is bounded above by

$$\Delta H \leq \frac{\Lambda_{\max} - \Lambda_{\min}}{2}, \tag{1.4}$$

where $\Lambda_{\max}$ and $\Lambda_{\min}$ are the maximum and minimum eigenvalues of H. The difference between the largest and least eigenvalues, denoted by

$$\|H\| = \Lambda_{\max} - \Lambda_{\min}, \tag{1.5}$$

is an operator seminorm of H. Using this seminorm, we can write a state-independent version of the QCRB [22],

$$\delta\gamma \geq \frac{1}{\sqrt{\nu}} \frac{1}{t\|H\|}. \tag{1.6}$$

This bound can be achieved by using the initial state $(|\Lambda_{\max}\rangle + |\Lambda_{\min}\rangle)/\sqrt{2}$, which evolves after time t to

*sflammia@perimeterinstitute.ca

$$e^{-iH\gamma t}\frac{1}{\sqrt{2}}(|\Lambda_{\max}\rangle + |\Lambda_{\min}\rangle)$$

$$= \frac{1}{\sqrt{2}}(e^{-i\Lambda_{\max}\gamma t}|\Lambda_{\max}\rangle + e^{-i\Lambda_{\min}\gamma t}|\Lambda_{\min}\rangle). \quad (1.7)$$

Measurement in a basis that includes the states $|\pm\rangle = (|\Lambda_{\max}\rangle \pm |\Lambda_{\min}\rangle)/\sqrt{2}$ yields outcomes ± 1 with probabilities $p_+ = \cos^2(\|H\|\gamma t/2)$ and $p_- = \sin^2(\|H\|\gamma t/2)$. Letting σ denote an observable with the outcome values ± 1, we have $\langle\sigma\rangle = \cos(\|H\|\gamma t)$ and $\Delta\sigma = |\sin(\|H\|\gamma t)|$. An appropriate estimator is defined in terms of the mean of the outcomes,

$$\frac{1}{\nu}\sum_{k=1}^{\nu}\sigma_k \equiv \cos(\|H\|\gamma_{\text{est}}t)$$

$$= \cos(\|H\|\gamma t) - \|H\|t\,\sin(\|H\|\gamma t)(\gamma_{\text{est}} - \gamma), \quad (1.8)$$

where the second expression is the linear approximation to the relation between γ_{est} and the mean of the outcomes, holding statistically in the limit of a large number of trials, specifically, $\nu \gg \tan^2(\|H\|\gamma t)$. Now it is easy to see that $\langle\gamma_{\text{est}}\rangle = \gamma$ and

$$\delta\gamma = \langle(\gamma_{\text{est}} - \gamma)^2\rangle^{1/2} = \frac{\Delta\sigma}{\sqrt{\nu}}\frac{1}{\|H\|t|\sin(\|H\|\gamma t)|} = \frac{1}{\sqrt{\nu}}\frac{1}{t\|H\|}, \quad (1.9)$$

showing that the bound (1.6) can be achieved and thus making it the fundamental limit to quantum metrology.

The $\sqrt{\nu}$ factor in Eqs. (1.3) and (1.6) is the well-understood statistical improvement available from averaging over many probes. In the remainder of the paper, we sometimes do not include this factor explicitly, referring to the remaining term on right-hand side of Eq. (1.3) or Eq. (1.6) as the QCRB, always remembering, of course, that generally the bound can only be achieved asymptotically in the limit of large ν.

It is clear from Eqs. (1.3) and (1.6) that strategies for improving the precision in estimating a parameter include changing the initial state of the probe, the coupling Hamiltonian H, or both. The case that has received most attention in the past is the one in which the probe constituents are coupled independently to the parameter,

$$H = \sum_{j=1}^{n} h_j. \quad (1.10)$$

Here h_j is a single-body operator acting on the jth constituent of the probe (hence, all these operators commute). In this case, the QCRB (1.6) scales like $\delta\gamma = O(1/n)$, a scaling known as the *Heisenberg limit* [1,10]. This scaling outperforms that attainable with classical statistics, which goes as $\delta\gamma = O(1/\sqrt{n})$, a scaling known as the *standard quantum limit* or, sometimes, as the *shot-noise limit*. The $1/\sqrt{n}$ scaling is the optimum sensitivity allowed by the QCRB (1.3) when the coupling Hamiltonian has the form (1.10) and the optimization of the probe state is restricted to product states.

Achieving the quantum-enhanced Heisenberg sensitivity with the linear coupling Hamiltonian (1.10) requires the probe to be initialized in a highly entangled state, which is a formidable challenge using current technology [1]. Much progress has been made in preparing such states toward precisely this end, e.g., by using measurement-induced squeezing [26], but it is still currently infeasible to use Heisenberg-limited experiments to outperform the best measurements operating at the standard quantum limit, although Heisenberg-like scalings have been achieved in related serial protocols that involve repeated interactions with a single constituent and thus do not involve entanglement [27]. Practical proposals [28] for reaching the Heisenberg limit have also been made in the context of measurements on a harmonic oscillator prepared in a state that displays sub-Planck phase-space structure [29].

More general families of Hamiltonians, containing nonlinear couplings of the constituents to the parameter, in contrast to the independent, linear coupling of Eq. (1.10), can perform better than the $1/n$ scaling of the Heisenberg limit, while respecting the QCRB [6,9,11,12,14,15,18]. In particular, when the coupling Hamiltonian has symmetric k-body terms in it, it is possible to achieve the scaling $\delta\gamma = O(n^{-k})$, as shown in [12]. This $O(n^{-k})$ scaling requires entangled input states, but we will show here that the optimal scaling with initial product states is $O(n^{-k+1/2})$. Thus scalings better than the $1/n$ Heisenberg scaling are possible for $k \geq 2$, even with initial product states for the probe, a result found for $k=2$ in [6,9,18].

In this paper we investigate the theoretical and practical bounds on precision in the generalized quantum metrology scheme introduced in [12], which allows for nonlinear couplings of the probe constituents to the parameter. In particular, we study the nonlinear coupling Hamiltonian [12]

$$H = \left(\sum_{j=1}^{n} h_j\right)^k = \sum_{a_1,\ldots,a_k}^{n} h_{a_1}\cdots h_{a_k}. \quad (1.11)$$

For simplicity, we assume that the probe constituents are identical and that the single-body operators h_j are the same for all the constituents. We review in Sec. II the optimal precision that can be achieved when the probe can be prepared in any initial state, particularly, entangled states of the probe constituents, but our emphasis in this paper is on the precision that can be attained when the initial state is restricted to be a product state.

In Sec. III we show that the optimal precision with product-state inputs scales as $O(n^{-k+1/2})$, and we find the corresponding optimal input state for the probe constituents. The sensitivity that can be achieved in practice depends, as mentioned above, on the measurements that are performed on the probe to extract information about γ. By analyzing the short-time limit, we show in Sec. IV that when the probe is initialized in a product state, simple, separable measurements on the probe constituents can achieve the optimal sensitivity. The conclusion, reached in [6,9,18] for specific cases, is that scalings better than the standard quantum limit—indeed, better than the Heisenberg limit—can be had without the need to invest in the generation of fragile initial entangled states. Our scheme thus circumvents a major bottleneck in attaining, in practice, scalings superior to $1/\sqrt{n}$.

In Sec. V, we analyze in detail a quadratic coupling Hamiltonian ($k=2$) for effective qubits, with $h_j=Z_j/2$, where Z_j is the Pauli z operator for the jth qubit. This case can be implemented in Bose-Einstein condensates [15,18], as was suggested in [12], and in fermionic atoms in optical lattices [15]. We show that the optimal sensitivity for input product states, scaling as $O(n^{-3/2})$, can be achieved by using the optimal product-state input found in Sec. III and making separable measurements of equatorial components of the total angular momentum of the effective qubits. Moreover, we show that, as was found independently in [18], the $O(n^{-3/2})$ scaling is attainable with these measurements starting with almost any state of the constituents except the equatorial states, which were the subject of the analysis in [15]. We formulate a simple model, based on the evolution of angular-momentum coherent states, that explains the origin of the $O(n^{-3/2})$ scaling. The model indicates that the entanglement generated by the quadratic Hamiltonian does not play a role in the enhanced sensitivity, and it suggests that, unlike protocols based on the use of entangled inputs, the product-state scheme should not be extremely sensitive to decoherence. We verify this suggestion by a brief analysis of the effect of phase decoherence in Sec. V B.

Section VI concludes with a brief summary of our results, including an extension of the coherent-state model to arbitrary k, and a discussion of our perception of the field of quantum-enhanced metrology.

II. GENERALIZED QUANTUM METROLOGY AND THE QUANTUM CRAMÉR-RAO BOUND

Attaining the QCRB (1.6) requires using an appropriate initial state and making appropriate measurements to extract the information about γ, but changing the optimal scaling with n requires changing the dependence of the coupling Hamiltonian H on n. This can be done by replacing the linear coupling Hamiltonian (1.10), which has just n terms, with the nonlinear Hamiltonian (1.11). The coupling Hamiltonian (1.11) describes a system with symmetric k-body couplings, including self-interactions, and it has n^k terms. For example, if the constituents are spin-$\frac{1}{2}$ particles and the operator h_j is the z component of the jth particle's spin, then H describes a coupling of the parameter to the kth power of the z component of the total angular momentum.

The eigenvectors of H are products of the eigenvectors of the h_j's. The eigenvectors can be labeled by a vector of single-body eigenvalues, $|\boldsymbol{\lambda}\rangle \equiv |\lambda_1,\ldots,\lambda_n\rangle$. The corresponding eigenvalues of h are given by the polynomial

$$\Pi_k(\boldsymbol{\lambda}) = \langle \boldsymbol{\lambda}|H|\boldsymbol{\lambda}\rangle = \left(\sum_{j=1}^{n}\lambda_j\right)^k = \sum_{a_1,\ldots,a_k}^{n}\lambda_{a_1}\cdots\lambda_{a_k}, \quad (2.1)$$

which is symmetric under permutation of its arguments and is known in the mathematical literature as the kth-degree elementary symmetric polynomial (on n variables).

To calculate the QCRB (1.6) for the k-body coupling Hamiltonian (1.11), we must calculate the maximum and minimum eigenvalues of H in terms of the eigenvalues of the single-body operators h_j, the total number of constituents n, and the degree of the coupling k. Let $\lambda_{\max}$ and $\lambda_{\min}$ be the largest and smallest eigenvalues of h_j. We consider four cases.

(1) k odd. The largest (smallest) eigenvalue of H is $\Lambda_{\max}=(n\lambda_{\max})^k$ [$\Lambda_{\min}=(n\lambda_{\min})^k$], corresponding to the eigenvector $|\Lambda_{\max}\rangle=|\lambda_{\max},\ldots,\lambda_{\max}\rangle$ ($|\Lambda_{\min}\rangle=|\lambda_{\min},\ldots,\lambda_{\min}\rangle$).

(2) k even, $\lambda_{\min}\geq 0$. The same conclusions apply as in case (1).

(3) k even, $\lambda_{\max}\leq 0$. The same conclusions apply as in case (2), except that the roles of $\lambda_{\max}$ and $\lambda_{\min}$ are reversed: the largest (smallest) eigenvalue, $\Lambda_{\max}=(n\lambda_{\min})^k$ [$\Lambda_{\min}=(n\lambda_{\max})^k$], corresponds to the eigenvector that has every constituent in the state $|\lambda_{\min}\rangle$ ($|\lambda_{\max}\rangle$).

(4) k even, $\lambda_{\min}<0<\lambda_{\max}$. Since all the eigenvalues of H are non-negative, the maximum eigenvalue is $\Lambda_{\max}=(n|\lambda|_{\max})^k$, where $|\lambda|_{\max}\equiv\max\{|\lambda_{\max}|,|\lambda_{\min}|\}$, corresponding to all the constituents being in either $|\lambda_{\max}\rangle$ or $|\lambda_{\min}\rangle$. The minimum eigenvalue comes from the string $\boldsymbol{\lambda}$, perhaps containing all eigenvalues, that makes $\Pi_k(\boldsymbol{\lambda})$ as close to zero as possible.

In cases (1)–(3), the QCRB (1.6) takes the form

$$\delta\gamma \geq \frac{1}{tn^k|\lambda_{\max}^k-\lambda_{\min}^k|}, \quad (2.2)$$

displaying the $O(n^{-k})$ scaling found in [12].

Case (4) requires further discussion regarding $\Lambda_{\min}$. We can bound $\Lambda_{\min}$ from above by considering strings $\boldsymbol{\lambda}$ that contain only $\lambda_{\max}$ and $\lambda_{\min}$. If $\lambda_{\max}$ appears a fraction p of the time, the corresponding eigenvalue is

$$\Pi_k(\boldsymbol{\lambda}) = [np\lambda_{\max}+n(1-p)\lambda_{\min}]^k. \quad (2.3)$$

This eigenvalue can be minimized by making $p\lambda_{\max}+(1-p)\lambda_{\min}$ as close to zero as possible, i.e., by choosing

$$np = \left\lceil \frac{n|\lambda_{\min}|}{\|h\|} \right\rfloor, \quad (2.4)$$

where $\lceil x\rfloor$ denotes the nearest integer to x and $\|h\|=\lambda_{\max}-\lambda_{\min}$ is the seminorm of the single-particle operators. The resulting eigenvalue can be written as $\Pi_k(\boldsymbol{\lambda})=(\delta\|h\|)^k$, where $\delta\leq 1/2$ is the magnitude of the difference between $n|\lambda_{\min}|/\|h\|$ and the integer closest to it. The minimum eigenvalue can be written as

$$\Lambda_{\min} = [(\delta-\varepsilon)\|h\|]^k, \quad (2.5)$$

where ε ($0\leq\varepsilon\leq 1/2$) accounts for the fact that strings containing other eigenvalues of the h_j's can generally make $\Lambda_{\min}$ smaller. If the constituents are qubits, $\varepsilon=0$. Since $\|h\|/|\lambda|_{\max}\leq 2$, we have

$$\frac{\Lambda_{\min}}{\Lambda_{\max}} = \left(\frac{\delta-\varepsilon}{n}\frac{\|h\|}{|\lambda|_{\max}}\right)^k \leq n^{-k}. \quad (2.6)$$

The upshot is that for even k and $\lambda_{\min}<0<\lambda_{\max}$, the QCRB (1.6) is given by

$$\delta\gamma \geq \frac{1}{tn^k|\lambda|_{\max}^k}\frac{1}{1-\Lambda_{\min}/\Lambda_{\max}}. \tag{2.7}$$

Thus the symmetric k-body coupling leads to a QCRB scaling as $O(n^{-k})$ in all four cases.

A closely related k-body coupling Hamiltonian is the same as Eq. (1.11), except that the self-interaction terms are omitted, which might be more appropriate in some physical situations. We analyze this alternative k-body coupling Hamiltonian in Appendix A and show that it also leads to a $O(n^{-k})$ QCRB scaling when arbitrary input states are allowed.

Luis and collaborators [6,9] showed that $O(n^{-2})$ scalings can be achieved in principle using a Kerr-type optical nonlinearity, and Luis generalized these results to optical nonlinearities of arbitrary order in [14]. Reference [17] proposes a method for synthesizing a quadratic ($k=2$) Hamiltonian from a linear Hamiltonian by passing a light beam 2 times through an atomic medium and finds a $O(n^{-2})$ scaling for this method.

III. ATTAINABLE PRECISION WITH PURE PRODUCT STATES

A. General bound

The QCRB (1.6) gives the best possible measurement precision, but can only be achieved for an optimal probe initial state, i.e., one of the form $(|\Lambda_{\max}\rangle+e^{i\phi}|\Lambda_{\min}\rangle)/\sqrt{2}$, which the results of Sec. II show is typically highly entangled. In this section we obtain lower bounds on $\delta\gamma$ in the situation where the initial state is a pure product state,

$$|\Psi_0\rangle = |\psi_1\rangle \otimes \cdots \otimes |\psi_n\rangle; \tag{3.1}$$

for this purpose, we start from the state-dependent QCRB (1.3). Since all the one-body operators h_j in the coupling Hamiltonian are assumed to be identical, it is reasonable to expect that the optimal initial product state will have all constituents in the same state, but we do not assume this at the outset, instead allowing its moral equivalent to emerge from the analysis.

The trick to evaluating ΔH is to partition the unrestricted sum in Eq. (1.11), in which terms in the sum contain different numbers of duplicate factors, into sums such that each term has the same sort of duplicate factors. Thus we write

$$H = \sum_{(a_1,\ldots,a_k)} h_{a_1}\cdots h_{a_k} + \binom{k}{2}\sum_{(a_1,\ldots,a_{k-1})} h_{a_1}\cdots h_{a_{k-2}}h_{a_{k-1}}^2 + \cdots, \tag{3.2}$$

where a summing range with parentheses $(a_1,\ldots,a_l)$ denotes a sum over all l-tuples that have no two elements equal. The two sums in Eq. (3.2) are the leading- and subleading-order terms in an expansion in which successive sums have fewer terms. The first sum in Eq. (3.2), in which the terms have no duplicate factors, has $n!/(n-k)! = O(n^k)$ terms, and the second sum, in which one factor is duplicated in each term, has $n!/(n-k-1)! = O(n^{k-1})$ terms. The binomial coefficient multiplying the second sum accounts for the number of ways of choosing the factor that is duplicated. The next sums in the expansion, involving terms with factors h_j^3 and $h_j^2h_l^2$, have $n!/(n-k-2)! = O(n^{k-2})$ terms. These expansions require that $n \geq k$, which we assume henceforth, and the scalings we identify further require that $n \gg k$.

Given the expansion (3.2), the expectation value of H has the form

$$\langle H\rangle = \sum_{(a_1,\ldots,a_k)} \langle h_{a_1}\rangle\cdots\langle h_{a_k}\rangle + \binom{k}{2} \times \sum_{(a_1,\ldots,a_{k-1})} \langle h_{a_1}\rangle\cdots\langle h_{a_{k-2}}\rangle\langle h_{a_{k-1}}^2\rangle + O(n^{k-2}). \tag{3.3}$$

The expression for $\langle H^2\rangle$ follows by replacing k with $2k$:

$$\langle H^2\rangle = \sum_{(a_1,\ldots,a_{2k})} \langle h_{a_1}\rangle\cdots\langle h_{a_{2k}}\rangle + \binom{2k}{2}\sum_{(a_1,\ldots,a_{2k-1})} \langle h_{a_1}\rangle\cdots\langle h_{a_{2k-2}}\rangle\langle h_{a_{2k-1}}^2\rangle + O(n^{2k-2}). \tag{3.4}$$

The rest of the analysis is based on an artful switching between restricted and unrestricted sums. By changing the initial sum in Eq. (3.3) to an unrestricted sum, we can rewrite $\langle H\rangle$ to the required order as

$$\langle H\rangle = \sum_{a_1,\ldots,a_k} \langle h_{a_1}\rangle\cdots\langle h_{a_k}\rangle + \binom{k}{2}\sum_{(a_1,\ldots,a_{k-1})} \langle h_{a_1}\rangle\cdots\langle h_{a_{k-2}}\rangle\Delta h_{a_{k-1}}^2 + O(n^{k-2}). \tag{3.5}$$

Squaring this expression and changing the unrestricted sums back to restricted ones, again keeping only the leading- and subleading-order terms, gives

$$\langle H\rangle^2 = \sum_{(a_1,\ldots,a_{2k})} \langle h_{a_1}\rangle\cdots\langle h_{a_{2k}}\rangle + \binom{2k}{2}\sum_{(a_1,\ldots,a_{2k-1})} \langle h_{a_1}\rangle\cdots\langle h_{a_{2k-2}}\rangle\langle h_{a_{2k-1}}\rangle^2 + 2\binom{k}{2}\sum_{(a_1,\ldots,a_{2k-1})} \langle h_{a_1}\rangle\cdots\langle h_{a_{2k-2}}\rangle\Delta h_{a_{k-1}}^2 + O(n^{2k-2}). \tag{3.6}$$

We can now find $(\Delta H)^2$ by subtracting Eq. (3.6) from Eq. (3.4),

$$(\Delta H)^2 = k^2\sum_{(a_1,\ldots,a_{2k-1})} \langle h_{a_1}\rangle\cdots\langle h_{a_{2k-2}}\rangle\Delta h_{a_{k-1}}^2 + O(n^{2k-2}) = k^2\left(\sum_{j=1}^n \langle h_j\rangle\right)^{2(k-1)}\left(\sum_{j=1}^n \Delta h_j^2\right) + O(n^{2k-2}). \tag{3.7}$$

In the final form, we take advantage of the fact that in the now leading-order sum, we can convert the restricted sum to an unrestricted one.

To make the QCRB (1.3) as small as possible, we need to maximize the variance $(\Delta H)^2$ of Eq. (3.7). We can immediately see that for fixed expectation values $\langle h_j\rangle$, we should maximize the variances Δh_j^2, and this is done by using for each constituent a state that lies in the subspace spanned by $|\lambda_{\max}\rangle$ and $|\lambda_{\min}\rangle$. Letting p_j be the probability associated with $|\lambda_{\max}\rangle$ for the jth constituent, we have

$$x_j \equiv \langle h_j\rangle = p_j\lambda_{\max} + (1-p_j)\lambda_{\min} = \lambda_{\min} + p_j\|h\|,$$

$$\begin{aligned}\Delta h_j^2 &= p_j\lambda_{\max}^2 + (1-p_j)\lambda_{\min}^2 - x_j^2 \\ &= \|h\|^2 p_j(1-p_j) \\ &= (\lambda_{\max}-x_j)(x_j-\lambda_{\min}).\end{aligned} \tag{3.8}$$

Thus we should maximize

$$(\Delta H)^2 = k^2\left(\sum_{j=1}^{n} x_j\right)^{2(k-1)} \sum_{j=1}^{n} (\lambda_{\max}-x_j)(x_j-\lambda_{\min}) \tag{3.9}$$

within the domain defined by $\lambda_{\min}\le x_j\le\lambda_{\max}$, $j=1,\ldots,n$.

Discarding potential extrema of $(\Delta H)^2$ given by $0=\Sigma_j x_j$, since these either are minima or lie outside the relevant domain, we find that the conditions for extrema of $(\Delta H)^2$ imply immediately that $x_j=x$ (and thus $p_j=p$) for $j=1,\ldots,n$. Thus, the optimal states in the initial product state (3.1) have the form

$$|\psi_j\rangle = \sqrt{p}|\lambda_{\max}\rangle + e^{i\phi_j}\sqrt{1-p}|\lambda_{\min}\rangle. \tag{3.10}$$

The only possible difference between the states for different constituents is in the relative phase between $|\lambda_{\max}\rangle$ and $|\lambda_{\min}\rangle$.

Since the optimal constituent states live and evolve in a two-dimensional subspace, we can regard the constituents effectively as qubits, with standard basis states $|0\rangle=|\lambda_{\max}\rangle$ and $|1\rangle=|\lambda_{\min}\rangle$, serving as the basis for constructing Pauli operators X, Y, and Z. Restricted to this subspace, the operator h takes the form

$$h = \lambda_{\max}|0\rangle\langle 0| + \lambda_{\min}|1\rangle\langle 1| = \bar{\lambda}\mathbb{1} + \|h\|Z/2, \tag{3.11}$$

where $\bar{\lambda}\equiv(\lambda_{\max}+\lambda_{\min})/2$ is the arithmetic mean of the largest and smallest eigenvalues of h.

In the analyses in Secs. IV and V, we assume that all the constituents have zero relative phase ($\phi_j=0$), giving an initial state $|\Psi_\beta\rangle=|\psi_\beta\rangle^{\otimes n}$, where

$$|\psi_\beta\rangle = e^{-i\beta Y/2}|0\rangle = \cos(\beta/2)|0\rangle + \sin(\beta/2)|1\rangle,$$

$$p = \cos^2(\beta/2) = (1+\cos\beta)/2. \tag{3.12}$$

Here we describe the one-body state $|\psi_\beta\rangle$ in terms of the rotation angle β about the y axis that produces it from $|0\rangle$. The corresponding initial density operator is

$$\rho_\beta = |\Psi_\beta\rangle\langle\Psi_\beta| = \bigotimes_{j=1}^{n}\frac{1}{2}(\mathbb{1}_j + X_j\sin\beta + Z_j\cos\beta). \tag{3.13}$$

The variance of H now takes the simple form

$$\begin{aligned}(\Delta H)^2 &= k^2 n^{2k-1}\langle h\rangle^{2(k-1)}(\Delta h)^2 \\ &= k^2 n^{2k-1}x^{2(k-1)}(\lambda_{\max}-x)(x-\lambda_{\min}),\end{aligned} \tag{3.14}$$

which leads, in the QCRB (1.3), to a sensitivity that scales as $1/n^{k-1/2}$ for input product states. This should be compared with the $O(n^{-k})$ scaling that can be obtained by using initial entangled states [12]. Notice that for $k\ge 2$, the $O(n^{-k+1/2})$ scaling is better than the $1/n$ scaling of the Heisenberg limit, which is the best that can be achieved in the $k=1$ case even with entangled initial states.

The coupling Hamiltonian that has the self-interaction terms of Eq. (1.11) removed is analyzed in Appendix A. We show that for initial product states, this modified Hamiltonian has the same leading-order behavior in the variance of H; it thus has $O(n^{-k+1/2})$ scaling for initial product states and the same optimal product states as we now find for the coupling Hamiltonian (1.11).

B. Optimal product states

The problem of finding the optimal input product state is now reduced to maximizing the $2k$-degree polynomial

$$f(x) \equiv x^{2(k-1)}(\lambda_{\max}-x)(x-\lambda_{\min}) = x^{2(k-1)}[\|h\|^2/4 - (x-\bar{\lambda})^2] \tag{3.15}$$

with respect to the single variable $x=\langle h\rangle$ on the domain $\lambda_{\min}\le x\le\lambda_{\max}$. The condition for an extremum is

$$0 = f'(x) = 2x^{2k-3}\{(k-1)[\|h\|^2/4 - (x-\bar{\lambda})^2] - x(x-\bar{\lambda})\}. \tag{3.16}$$

We assume $k\ge 2$, because the $k=1$ case is already well understood. For $k=1$, there is a single maximum at $x=\bar{\lambda}$, corresponding to equal probabilities for $|\lambda_{\max}\rangle$ and $|\lambda_{\min}\rangle$ and to $(\Delta H)^2=n\|h\|^2/4$.

The polynomial f vanishes at $x=\lambda_{\min}$ and $x=\lambda_{\max}$. We can make some general statements about the extrema of f in three cases.

(1) If $\lambda_{\min}<0<\lambda_{\max}$, f has a minimum at $x=0$ and two maxima within the allowed domain, one at a positive $x_+>\bar{\lambda}$ and one at a negative $x_-<\bar{\lambda}$. The global maximum is at x_+ (x_-) if $|\lambda|_{\max}=\lambda_{\max}$ ($|\lambda|_{\max}=|\lambda_{\min}|$).

(2) If $\lambda_{\max}>\lambda_{\min}>0$, f has a maximum at $x=0$, a minimum for a positive $x_-<\lambda_{\min}$, and a maximum within the allowed domain at $x_+>\bar{\lambda}$. Only the last of these lies in the relevant domain.

(3) If $\lambda_{\min}<\lambda_{\max}<0$, f has a maximum at $x=0$, a minimum for a negative $x_+>\lambda_{\max}$, and a maximum within the allowed domain at $x_-<\bar{\lambda}$. Only the last of these lies in the relevant domain.

These general observations are perhaps more enlightening than the form of the (nonzero) solutions of Eq. (3.16),

$$x_\pm = \left(1-\frac{1}{2k}\right)\bar{\lambda} \pm \frac{1}{2}\sqrt{\frac{\bar{\lambda}^2}{k^2} + \left(1-\frac{1}{k}\right)\|h\|^2}. \tag{3.17}$$

The $\pm$ here means the same thing as in the discussion of the three cases above.

As k increases, x_+ approaches $\lambda_{\max}$, and x_- approaches $\lambda_{\min}$. Indeed, as $k\to\infty$, we have $x_+=(1-1/2k)\lambda_{\max}$, corresponding to $p_+=1-\lambda_{\max}/2k\|h\|$ and $(\Delta H)^2=(k/2e)\times(n\lambda_{\max})^{2k-1}\|h\|$, and $x_-=(1-1/2k)\lambda_{\min}$, corresponding to $p_-=-\lambda_{\min}/2k\|h\|$ and $(\Delta H)^2=(k/2e)(-n\lambda_{\min})^{2k-1}\|h\|$.

An important limiting case, not covered in the discussion above, occurs when $\lambda_{\min}=-\lambda_{\max}$. Then the maxima occur symmetrically at

$$x_\pm = \pm\frac{1}{2}\|h\|\sqrt{1-1/k}, \tag{3.18}$$

corresponding to probabilities $p_\pm=\frac{1}{2}+x_\pm/\|h\|=\frac{1}{2}(1\pm\sqrt{1-1/k})=1-p_\mp$ and to $\sin\beta_\pm=\sqrt{1/k}$. The two maxima lead to the same variance,

$$(\Delta H)^2 = k(1-1/k)^{k-1}n^{2k-1}(\|h\|/2)^{2k}, \tag{3.19}$$

thus yielding a QCRB,

$$\delta\gamma \geq \frac{2^{k-1}}{k^{1/2}(1-1/k)^{(k-1)/2}}\frac{1}{tn^{k-1/2}\|h\|^k}. \tag{3.20}$$

Of course, when $\lambda_{\min}=-\lambda_{\max}$, we can always choose units such that $\lambda_{\max}=1/2$ ($\|h\|=1$), which means that the single-body operators are $h_j=Z_j/2$. It is this situation that we analyze in the remainder of this paper.

IV. SEPARABLE MEASUREMENTS

In the preceding section we obtained the theoretical limits on the measurement uncertainty with symmetric k-body couplings and initial product states for the probe. The theoretical bound is saturated by a measurement of the so-called symmetric logarithmic derivative [22–25]; this measurement, in general, is entangled and depends on the value of the parameter that we are attempting to estimate. In this section we show that for some Hamiltonians of interest, standard separable measurements lead to uncertainties for small γ that have the same scaling as the theoretical bounds. The restriction to small values of γ is not a strong limitation, because we can always use feedback to operate in this regime, as we discuss in more detail in Sec. V A.

We consider the special case in which the single-body operators are $h_j=Z_j/2$, leading to a coupling Hamiltonian

$$H = \left(\sum_j \frac{Z_j}{2}\right)^k = J_z^k. \tag{4.1}$$

Here we introduce J_z as the z component of a "total angular momentum" corresponding to the effective qubits. We assume an initial state of the form (3.13), and we let this state evolve for a very short time, i.e., $\phi\equiv\gamma t\ll 1$. In the remainder of the paper, we often work in terms of the parameter ϕ instead of γ. After the time evolution, we measure the separable observable

$$J_y = \sum_j Y_j. \tag{4.2}$$

Over ν trials, we estimate ϕ as a scaled arithmetic mean of the results of the J_y measurements.

The expectation value of any observable at time t is given by

$$\langle M\rangle_t = \mathrm{Tr}(U^\dagger M U\rho_\beta) = \langle U^\dagger M U\rangle, \tag{4.3}$$

where $U=e^{-iH\gamma t}=e^{-iH\phi}$, and where we introduce the convention that an expectation value with no subscript is taken with respect to the initial state. For small ϕ, we have

$$U^\dagger M U = M - i\phi[M,H] + O(\phi^2). \tag{4.4}$$

Thus, the expectation value and variance of J_y at time t take the form

$$\langle J_y\rangle_t = \langle J_y\rangle - i\phi\langle[J_y,H]\rangle + O(\phi^2), \tag{4.5a}$$

$$(\Delta J_y)_t^2 = (\Delta J_y)_0^2 - i\phi\langle(J_y-\langle J_y\rangle)[J_y,H] + [J_y,H](J_y-\langle J_y\rangle)\rangle + O(\phi^2). \tag{4.5b}$$

The initial expectation value and variance of J_y are those of an angular-momentum coherent state in the x-z plane,

$$\langle J_y\rangle = 0, \tag{4.6a}$$

$$(\Delta J_y)_0^2 = \langle J_y^2\rangle = \frac{1}{4}\sum_{j,l}\langle Y_j Y_l\rangle = \frac{n}{4}. \tag{4.6b}$$

In evaluating the other expectation values in Eqs. (4.5), we can avail ourselves of the expansions used in Sec. III A, since we are only interested in the leading-order behavior in n. To leading order, the coupling Hamiltonian has the form

$$H = \frac{1}{2^k}\sum_{(a_1,\ldots,a_k)} Z_{a_1}\cdots Z_{a_k} + O(n^{k-1}). \tag{4.7}$$

In this section we use $\approx$, to indicate equalities that are good to leading order in n. We can now write

$$\begin{aligned}[J_y,H] &\approx \frac{1}{2^{k+1}}\sum_{j=1}^{n}\sum_{(a_1,\ldots,a_k)}[Y_j,Z_{a_1}\cdots Z_{a_k}]\\ &= \frac{i}{2^k}\sum_{l=1}^{k}\sum_{(a_1,\ldots,a_k)} Z_{a_1}\cdots Z_{a_{l-1}}X_{a_l}Z_{a_{l+1}}\cdots Z_{a_k}\\ &= \frac{ik}{2^k}\sum_{(a_1,\ldots,a_k)} X_{a_1}Z_{a_2}\cdots Z_{a_k},\end{aligned} \tag{4.8}$$

from which it follows that

$$\langle[J_y,H]\rangle \approx \frac{ik}{2^k}\sum_{(a_1,\ldots,a_k)}\langle X_{a_1}\rangle\langle Z_{a_2}\rangle\cdots\langle Z_{a_k}\rangle \approx ik\langle J_x\rangle\langle J_z\rangle^{k-1}. \tag{4.9}$$

Elaborating this procedure one step further, we can show that to leading order in n, the expectation value in the second term of Eq. (4.5b) vanishes. Our results to this point are summarized by

$$\begin{aligned}\langle J_y\rangle_t &\approx \phi k\langle J_x\rangle\langle J_z\rangle^{k-1} + O(\phi^2)\\ &= \phi k(n/2)^k\sin\beta\cos^{k-1}\beta + O(\phi^2),\end{aligned} \tag{4.10a}$$

$$(\Delta J_y)_t \approx \sqrt{n}/2 + O(\phi^2). \tag{4.10b}$$

If we let our estimator $\phi_{\rm est}$ be the arithmetic mean of the ν measurements of J_y, scaled by the factor $(d\langle J_y\rangle_t/d\phi)^{-1} = 1/k(n/2)^k \sin\beta\cos^{k-1}\beta$, we have

$$\langle\phi_{\rm est}\rangle = \frac{\langle J_y\rangle_t}{d\langle J_y\rangle_t/d\phi} \approx \phi + O(\phi^2), \tag{4.11}$$

$$\delta\phi \approx \frac{1}{\sqrt{\nu}}\frac{(\Delta J_y)_t}{|d\langle J_y\rangle_t/d\phi|} + O(\phi)$$
$$\approx \frac{1}{\sqrt{\nu}}\frac{2^{k-1}}{kn^{k-1/2}\sin\beta|\cos^{k-1}\beta|} + O(\phi). \tag{4.12}$$

This scheme thus attains the $O(n^{-k+1/2})$ scaling that is the best that can be achieved by initial product states. In an analysis of optical nonlinearities of arbitrary order, Luis [14] reported finding this $O(n^{-k+1/2})$ scaling.

The minimum of $\delta\phi$, occurring when $\sin\beta=\sqrt{1/k}$, gives an optimal sensitivity

$$\delta\phi \approx \frac{1}{\sqrt{\nu}}\frac{2^{k-1}}{k^{1/2}(1-1/k)^{(k-1)/2}}\frac{1}{n^{k-1/2}} + O(\phi), \tag{4.13}$$

which is identical to the optimal QCRB sensitivity for initial product states. For $k=2$, the case that is the subject of the next section, the two optimal values of β are $\beta=\pi/4$ and $\beta=3\pi/4$, and the sensitivity becomes

$$\delta\phi \approx \frac{1}{\sqrt{\nu}}\frac{2}{n^{3/2}} + O(\phi). \tag{4.14}$$

Aside from showing that the QCRB scaling for initial product states can be achieved, the analysis in this section serves to illustrate how the product-state scheme works in a regime that has a singularly simple description. The J_z^k coupling Hamiltonian induces a nonlinear rotation about the z axis, which rotates the probe through an angle $\langle J_y\rangle_t/\langle J_x\rangle \approx \phi k\langle J_z\rangle^{k-1}$. This rotation induces a signal in J_y of size $\approx\phi k\langle J_x\rangle\langle J_z\rangle^{k-1}$, which is $k\langle J_z\rangle^{k-1}$ times larger than for $k=1$, yet is to be detected against the same coherent-state uncertainty $\sqrt{n}/2$ in J_y as for $k=1$. To take advantage of the nonlinear rotation, we cannot make the J_x lever arm of the rotation as large as possible, because the nonlinear rotation vanishes when the initial coherent state lies in the equatorial plane. Nonetheless, we still win when we make the optimal compromise between the nonlinear rotation and the lever arm. The optimal compromise comes from maximizing $\langle J_x\rangle \times\langle J_z\rangle^{k-1}$, which turns out to be exactly the same as finding the optimum in the QCRB analysis of Sec. III B because $\langle X\rangle=\sin\beta=\Delta Z$.

A more careful consideration of the terms neglected in this analysis suggests that, as formulated in this section, the small-time approximation requires that $\phi\ll 1/n^{k-1}$. Nonetheless, the analysis is consistent because ϕ can be resolved more finely than this scale, i.e., $\delta\phi n^{k-1}=O(1/\sqrt{n})$. This conclusion is confirmed by the more detailed analysis of the $k=2$ case in Sec. V. On the other hand, the simple model of coherent-state evolution, developed for $k=2$ in Sec. V, suggests the description of the preceding paragraph can be extended to much larger times. We return to this point in Sec. VI.

V. SEPARABLE MEASUREMENTS FOR THE INTERACTION $H_\gamma=\gamma J_z^2$

We focus now on the symmetric, $k=2$ coupling Hamiltonian

$$H_\gamma = \gamma J_z^2 = \gamma\left(\sum_j \frac{Z_j}{2}\right)^2. \tag{5.1}$$

This is perhaps the most important example for practical applications of nonlinear Hamiltonians to quantum metrology [12], since it occurs naturally whenever the strength of two-body interactions is modulated by a parameter γ. As suggested in [12], one good place to look for this kind of coupling Hamiltonian is in Bose-Einstein condensates. Indeed, in [15,18], it is shown how this Hamiltonian can be implemented using the internal atomic states of BECs. In analyzing the BEC scenario, Ref. [15] finds a sensitivity that scales as $O(1/n)$ for separable measurements made on a probe that evolves from an initial product state chosen to be an angular-momentum coherent state in the equatorial plane. The results in the preceding sections show that we should be able to improve this scaling to $O(n^{-3/2})$ through a wiser choice of the initial coherent state. In this section we analyze this situation in some detail.

We take the initial state of the n-qubit probe to be an angular-momentum coherent state that is at an angle β from the z axis in the x-z plane. This state is obtained from the coherent state along the z axis, $|J,J\rangle=|0\rangle^{\otimes n}$, by a rotation through β about the y axis,

$$|\Psi_\beta\rangle = e^{-i\beta J_y}|J,J\rangle = (e^{-i\beta Y/2}|0\rangle)^{\otimes n}. \tag{5.2}$$

The rotation about the y axis and the nonlinear rotation under the interaction Hamiltonian (5.1) both leave the state in the $(2J+1)$-dimensional subspace with angular momentum $J=n/2$, so we can use the basis $|J,m\rangle$ of J_z eigenstates for this subspace, with $m=-J,\ldots,J$. The initial probe state used in [15] is a special case, $\beta=-\pi/2$.

The state $|\Psi_\beta\rangle=\Sigma_{m=-J}^{J} d_m|J,m\rangle$, can be expanded in the basis $|J,m\rangle$ using a reduced Wigner rotation matrix [30]

$$d_m \equiv d^J_{mJ}(\beta) = \langle J,m|e^{-i\beta J_y}|J,J\rangle$$
$$= \sqrt{\frac{(2J)!}{(J+m)!\,(J-m)!}}[\cos(\beta/2)]^{J+m}[\sin(\beta/2)]^{J-m}. \tag{5.3}$$

At time $t=\phi/\gamma$, the state of the probe becomes

$$|\Psi_\beta(t)\rangle = e^{-i\phi J_z^2}|\Psi_\beta\rangle = \sum_{m=-J}^{J} d_m e^{-i\phi m^2}|J,m\rangle. \tag{5.4}$$

A. Measurements

We now look at the attainable measurement uncertainties using both $J_x=\Sigma X_j/2$ and $J_y=\Sigma_j Y_j/2$ measurements on the

final state of the probe. It turns out that J_x and J_y measurements are on nearly the same footing, with J_y measurements being marginally better, for all β except $\beta=\pi/2$. For very short times, the superiority of J_y measurements for $\beta\neq\pi/2$ is clear from the analysis in Sec. IV, since the change in $\langle J_y\rangle$ is linear in ϕ, whereas the change in $\langle J_x\rangle$ is quadratic. What happens for longer times and for $\beta=\pi/2$ cannot be addressed by the short-time analysis in Sec. III. What we find in this section is that both J_x and J_y measurements can achieve the optimal scaling obtained in Sec. III. For $\beta=\pi/2$, J_y measurements provide no information about ϕ, but J_x measurements achieve the $O(n^{-1})$ scaling found in [15]. These conclusions assume no decoherence, and in Sec. V B we explore the impact of decoherence on the ability to achieve super-Heisenberg scalings with the symmetric, $k=2$ coupling Hamiltonian.

For measurements of J_x or J_y, the sensitivity is given by

$$\delta\phi_{x,y}=t\delta\gamma_{x,y}=\frac{(\Delta J_{x,y})_\phi}{|d\langle J_{x,y}\rangle_\phi/d\phi|} \tag{5.5}$$

(for this section, we revert to our practice of omitting the $1/\sqrt{\nu}$ statistical factor from our sensitivity formulas).

The expressions needed to calculate $\delta\phi$ for J_x and J_y measurements are derived in Appendix B. These results are conveniently expressed in terms of the raising and lowering operators

$$J_\pm=J_x\pm iJ_y, \tag{5.6}$$

since we can write

$$\langle J_x\rangle_\phi=\mathrm{Re}(\langle J_+\rangle_\phi),\quad \langle J_y\rangle_\phi=\mathrm{Im}(\langle J_+\rangle_\phi), \tag{5.7}$$

$$\langle J_{x,y}^2\rangle_\phi=\frac{1}{4}\langle J_+J_-+J_-J_+\rangle_\phi\pm\frac{1}{2}\mathrm{Re}(\langle J_+^2\rangle_\phi), \tag{5.8}$$

where the upper sign in Eq. (5.8) applies to J_x and the lower sign to J_y. In Appendix B, we show that

$$\begin{aligned}\langle J_+\rangle_\phi&=J\sin\beta(\cos\phi+i\sin\phi\cos\beta)^{2J-1}\\&=J\sin\beta r^{2J-1}e^{i(2J-1)\theta},\end{aligned} \tag{5.9}$$

$$\frac{1}{2}\langle J_+J_-+J_-J_+\rangle_\phi=J+\frac{J(2J-1)}{2}\sin^2\beta, \tag{5.10}$$

$$\begin{aligned}\langle J_+^2\rangle_\phi&=\frac{J(2J-1)}{2}\sin^2\beta(\cos 2\phi+i\sin 2\phi\cos\beta)^{2(J-1)}\\&=\frac{J(2J-1)}{2}\sin^2\beta R^{2(J-1)}e^{2i(J-1)\Theta},\end{aligned} \tag{5.11}$$

where

$$r=(1-\sin^2\phi\sin^2\beta)^{1/2}, \tag{5.12a}$$

$$\theta=\tan^{-1}(\tan\phi\cos\beta), \tag{5.12b}$$

and

$$R=(1-\sin^2 2\phi\sin^2\beta)^{1/2}, \tag{5.13a}$$

$$\Theta=\tan^{-1}(\tan 2\phi\cos\beta). \tag{5.13b}$$

Plugging these results into Eqs. (5.7) and (5.8), we arrive at

$$\langle J_x\rangle_\phi=J\sin\beta r^{2J-1}\cos[(2J-1)\theta], \tag{5.14}$$

$$\langle J_y\rangle_\phi=J\sin\beta r^{2J-1}\sin[(2J-1)\theta], \tag{5.15}$$

and

$$\langle J_{x,y}^2\rangle_\phi=\frac{J}{2}+\frac{J(2J-1)}{4}\sin^2\beta\{1\pm R^{2(J-1)}\cos[2(J-1)\Theta]\}. \tag{5.16}$$

In using these results in what follows, it is easier to deal directly with the first forms in Eqs. (5.9) and (5.11) rather than working with the functions r, θ, R, and Θ.

The expectation values $\langle J_{x,y}\rangle_\phi$ change sign when ϕ advances by π. This means that their squares and absolute values, which are all that appear in the sensitivity (5.5), are periodic with period π. The second moments $\langle J_{x,y}^2\rangle_\phi$ are periodic with period $\pi/2$. The upshot is that the uncertainties $\Delta J_{x,y}$ and the precision $\delta\phi_{x,y}$ are periodic with period π. This π periodicity is a consequence of periodic revivals in the evolved state $|\Psi_\beta(t)\rangle$.

The main features of the sensitivity $\delta\phi$ for measurements of J_x and J_y can be gleaned from Fig. 1. It is clear from these plots that the best sensitivity is achieved when ϕ is near zero and also, because of the periodicity of $\delta\phi$, when ϕ is near $q\pi$, for q any integer.

When J is large, we can develop a good approximation for the entire region of high sensitivity, where ϕ is small, by writing

$$(\cos\phi+i\sin\phi\cos\beta)^{2J-1}\simeq e^{2iJ\phi\cos\beta}e^{-J\phi^2\sin^2\beta}, \tag{5.17a}$$

$$(\cos 2\phi+i\sin 2\phi\cos\beta)^{2(J-1)}\simeq e^{4iJ\phi\cos\beta}e^{-4J\phi^2\sin^2\beta}. \tag{5.17b}$$

These approximations are good to second order in ϕ in the exponent. When ϕ is near $q\pi$, the same approximations can be had by replacing ϕ with $\phi-q\pi$. The complex exponentials give rise to rapidly oscillating fringes in $\langle J_{x,y}\rangle_\phi$ and $\langle J_{x,y}^2\rangle_\phi$, with periods $\sim 1/J\cos\beta$; the slower Gaussian envelopes take these expressions to zero when ϕ is a few times $|\sin\beta|/\sqrt{J}$.

It is not hard to work out the sensitivity in this approximation, but the formulas are sufficiently messy that they are little more illuminating than the exact expressions. We can, however, develop a very simple, yet instructive picture of the fringes by keeping them, but assuming that ϕ is small enough that the Gaussian envelopes have yet to become effective, i.e., $\sqrt{J}\phi\sin\beta$ is somewhat smaller than 1. In this approximation, the fringes are uniform in ϕ, and we obtain

$$\langle J_x\rangle_\phi\simeq J\sin\beta\cos(2J\phi\cos\beta), \tag{5.18}$$

$$\langle J_y\rangle_\phi\simeq J\sin\beta\sin(2J\phi\cos\beta), \tag{5.19}$$

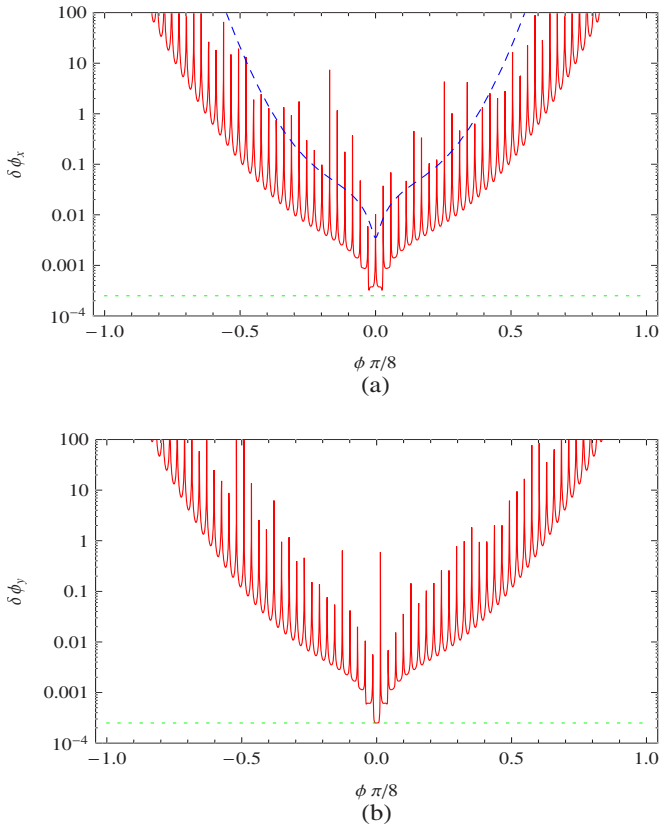

FIG. 1. (Color online) Sensitivity (solid red lines) vs ϕ ($-\pi/8 \le \phi \le \pi/8$) using an optimal initial state at angle $\beta=\pi/4$: (a) J_x measurements; (b) J_y measurements. The total angular momentum J of the probe is 200, corresponding to $n=400$. The lower bound on the sensitivity, $1/\sqrt{2}J^{3/2}$, is plotted as the dotted (green) line. The sensitivity is characterized by rapidly oscillating fringes and a decay of sensitivity away from the best sensitivities near $\phi=0$. The sensitivity patterns repeat with periodicity π; only one-quarter of a period is plotted because the sensitivity worsens even more outside the plotted region. Part (a) also shows the sensitivity for J_x measurements when $\beta=\pi/2$ (dashed blue line); notice the absence of fringes in this case and the substantially degraded sensitivity.

$$(\Delta J_x)^2_\phi \simeq \frac{J}{2}[1-\sin^2\beta\cos^2(2J\phi\cos\beta)], \tag{5.20}$$

$$(\Delta J_y)^2_\phi \simeq \frac{J}{2}[1-\sin^2\beta\sin^2(2J\phi\cos\beta)]. \tag{5.21}$$

These lead to sensitivities

$$\delta\phi_x^2 \simeq \frac{1}{2J^3}\frac{1-\sin^2\beta\cos^2(2J\phi\cos\beta)}{\sin^2 2\beta\sin^2(2J\phi\cos\beta)}, \tag{5.22}$$

$$\delta\phi_y^2 \simeq \frac{1}{2J^3}\frac{1-\sin^2\beta\sin^2(2J\phi\cos\beta)}{\sin^2 2\beta\cos^2(2J\phi\cos\beta)}. \tag{5.23}$$

Within this uniform-fringe approximation, the best sensitivities are achieved at the troughs of the fringes: the best operating points are, for J_x measurements,

$$\phi = q\pi + \frac{(s+1/2)\pi}{2J\cos\beta}, \tag{5.24}$$

and for J_y measurements,

$$\phi = q\pi + \frac{s\pi}{2J\cos\beta}, \tag{5.25}$$

where q and s are integers. At these operating points, the sensitivity for both measurements becomes

$$\delta\phi_{x,y} \simeq \frac{1}{\sqrt{2}J^{3/2}|\sin 2\beta|}, \tag{5.26}$$

which takes on its optimal value, $1/\sqrt{2}J^{3/2}=2/n^{3/2}$, when $\beta=\pi/4$ or $\beta=3\pi/4$, in agreement with the analyses in Secs. III and IV. This $O(J^{-3/2})$ scaling has been found independently by Choi and Sundaram [18] and for nonlinear optical systems by Luis and collaborators [6,9]. For $\beta=\pi/4$ and $J=2500$, Fig. 2 plots the central fringes of the approximate sensitivities (5.22) and (5.23) and compares them with the exact sensitivities and the Gaussian approximation for measurements of J_x and J_y.

As we show in Appendix B, within the uniform-fringe approximation, the evolved state (5.4) is an angular-momentum coherent state that makes an angle β with the z axis and that rotates around the z axis with angular velocity $2\gamma J\cos\beta$. The enhanced sensitivity available from a quadratic Hamiltonian is a consequence of this increased rotation rate, which is greater by a factor of $2J\cos\beta=2\langle J_z\rangle$ than that available from a linear Hamiltonian. This same conclusion came out of the short-time analysis of Sec. IV, but it is stronger now because the uniform-fringe approximation is much better than the short-time approximation. The short-time approximation requires that $J\phi \ll 1$ and thus describes correctly only the center of the central fringe for J_y measurements. In contrast, the uniform-fringe approximation only requires that $\phi\sqrt{J}|\sin\beta| \ll 1$; within this requirement, there can be several fringes, i.e., $2J\phi\cos\beta$ can be somewhat larger than π, provided that $J \gg \tan^2\beta$. The more accurate uniform-fringe approximation allows us to see the other near-optimal operating points for J_y measurements and to see the optimal operating points for J_x measurements, which lie not at $\phi=0$, but at $\phi=\pm\pi/4J\cos\beta$. As β approaches $\pi/2$, the fringes become wider and wider, making the uniform-fringe approximation reliable only for larger and larger values of J. For $\beta=\pi/2$, the fringes disappear entirely, and a separate analysis is required to find the scaling for J_x measurements (since $\langle J_y\rangle_\phi=0$ for $\beta=\pi/2$, measurements of J_y provide no information about ϕ).

That the final state (5.4), within the region of high sensitivity, is approximately an angular-momentum coherent state tells us two important things. First, even though the quadratic Hamiltonian will generate entanglement from a product state, this entanglement plays no role in the enhanced sensitivity. The improved sensitivity comes from the increased rotation rate of the coherent state, which is a product state, having no entanglement among the probe constituents. Indeed, for the measurements we consider here, the deviation from being a coherent state makes the sensitivity worse. Sec-

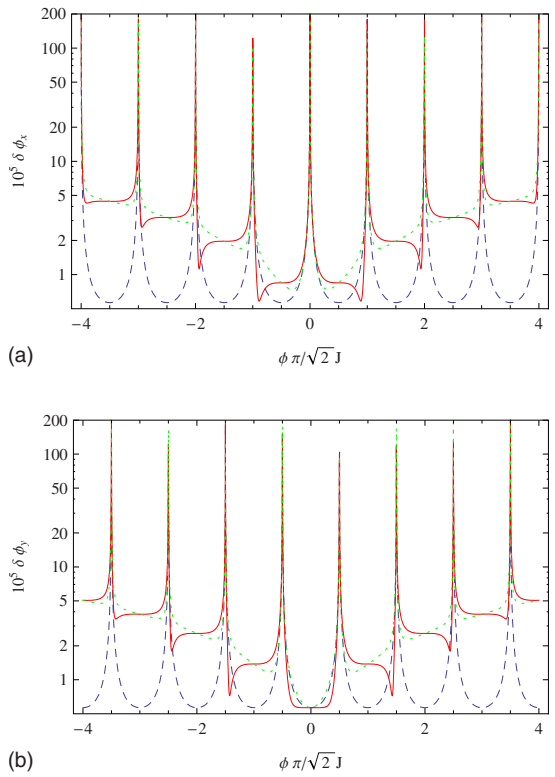

FIG. 2. (Color online) Central few fringes of the measurement precision for $\beta=\pi/4$ and $J=2500$ $(n=5000)$: (a) J_x measurements; (b) J_y measurements. The solid (red) lines are the exact sensitivities, the dashed (blue) lines are the sensitivities given by the uniform-fringe approximation of Eqs. (5.22) and (5.23), $\delta\phi_x \simeq (1/2J^{3/2})\sqrt{1+[1/\sin^2(2J\phi\cos\beta)]}$, $\delta\phi_y \simeq (1/2J^{3/2})\sqrt{1+[1/\cos^2(2J\phi\cos\beta)]}$, and the dotted (green) lines are the Gaussian-envelope approximation of Eqs. (5.17). The uniform-fringe approximation locates the fringes precisely, but misses entirely the degradation in sensitivity as one moves away from the central fringes and also fails to characterize accurately the shape of the fringes. The Gaussian-envelope approximation improves on this performance by capturing the degradation of sensitivity quite well, but still fails on the fringe shapes. Even the central fringe for J_y measurements is noticeably flatter than in the two approximations. To get the best sensitivity, one should operate right on the central fringe, at $\phi=q\pi$, for J_y measurements and on one of the two central fringes, centered at $\phi=q\pi\pm\pi/4J\cos\beta$ for J_x measurements. Notice that J_x measurements achieve nearly optimal sensitivity at points near the outside of these two central fringes.

ond, that the probe state is approximately a product state within the region of high sensitivity hints that this scheme should not be as fragile in the presence of decoherence as schemes that rely on initial entanglement. We investigate the impact of decoherence in Sec. V B and show that the $O(n^{-3/2})$ scaling is unaffected by phase decoherence.

To achieve the optimal sensitivity for J_x or J_y measurements, we need to operate within the appropriate central fringe, of width $\pi/\sqrt{2}J$ for $\beta=\pi/4$. This can be done by using an adaptive feedback procedure, which we discuss in the context of J_y measurements. The feedback procedure is carried out in several steps, in each of which the quantity that is estimated is $\phi-\phi_{\mathrm{est}}$, where ϕ_{est} is the estimate of ϕ from the previous step. At each step, we choose $J=n/2$ so that $\phi-\phi_{\mathrm{est}}$ is with very high probability close to the center of the central fringe, and we use ν probes to determine ϕ with greater precision for the next step. As we obtain progressively refined estimates of ϕ, the quantity being estimated becomes smaller and smaller, always lying well within a sequence of progressively finer central fringes.

To check that this procedure works and to determine its scaling properties, imagine that we determine $\phi/2\pi$ bit by bit. At step l, we determine the lth bit of $\phi/2\pi$ by choosing $J=J_l$ so that the precision is given by

$$\frac{\delta\phi_l}{2\pi}=\frac{1}{\sqrt{\nu}}\frac{1}{2\pi\sqrt{2}J_l^{3/2}}=\frac{1}{f2^l}, \tag{5.27}$$

where the factor $f\sim 3-10$ is chosen to ensure that we get the right lth bit with very high probability. This gives

$$J_l=\frac{1}{2\nu^{1/3}}\left(\frac{f2^l}{\pi}\right)^{2/3}. \tag{5.28}$$

We must, of course, choose J_l to be an integer or half-integer, so we choose the nearest one, but this detail does not change the resource calculation significantly, so we ignore it. At step $l+1$, $\phi-\phi_{\mathrm{est}}$ lies well within the central fringe, as we see from

$$\frac{\delta\phi_l}{\pi/\sqrt{2}J_{l+1}}=\frac{2^{7/6}}{\pi\nu^{1/3}}\left(\frac{\pi}{f2^l}\right)^{1/3}. \tag{5.29}$$

Indeed, because of the $O(J^{-3/2})$ scaling, the quantity being estimated is buried progressively deeper fractionally in the central fringe as we step through the procedure, despite the fact that the central fringe is itself narrowing exponentially.

Suppose now that we use this procedure to estimate L bits of ϕ. The total number of constituents used,

$$N=\nu\sum_{l=1}^{L}2J_l=\left(\frac{2\nu f}{\pi}\right)^{2/3}\frac{2^{2L/3}-1}{2^{2/3}-1}, \tag{5.30}$$

is dominated by the last step, as is typical in these feedback procedures. The ultimate precision displays the $O(N^{-3/2})$ scaling,

$$2\pi 2^{-L}=\frac{4f}{(2^{2/3}-1)^{3/2}}\frac{\nu}{N^{3/2}}=\frac{2f}{(2^{2/3}-1)^{3/2}}\frac{1}{\sqrt{\nu}}\frac{2}{(N/\nu)^{3/2}}, \tag{5.31}$$

with a small additional overhead given by the factor $2f/(2^{2/3}-1)^{3/2}$.

As β becomes smaller, the uniform-fringe approximation becomes progressively better, since the fringes oscillate rapidly and the Gaussian envelopes become very broad. On the other hand, the signal in J_x and J_y disappears, making the sensitivity worsen as $1/\sin^2 2\beta$.

At the other extreme, as β approaches $\pi/2$, the uniform-fringe approximation becomes poorer as the fringes become as wide as the Gaussian envelopes and loses validity entirely when $J|\cot\beta|\sim 1$. When $\beta=\pi/2$, which is the initial probe state analyzed by Rey *et al.* [15] (Ref. [15] actually uses $\beta=-\pi/2$, but this state is equivalent to $\beta=\pi/2$ for purposes of

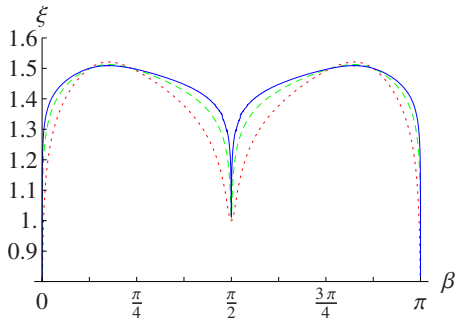

FIG. 3. (Color online) Scaling exponent ξ for J_x measurements. The dotted (red) line is for $J=10^3$, the dashed (green) line for $J=10^5$, and the solid (blue) line for $J=10^7$.

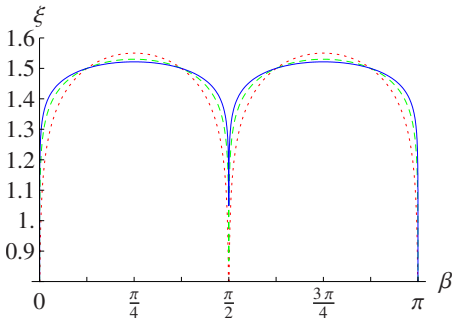

FIG. 4. (Color online) Scaling exponent ξ for J_y measurements. The dotted (red) line is for $J=10^3$, the dashed (green) line for $J=10^5$, and the solid (blue) line for $J=10^7$.

these measurements), $|J_y\rangle_\phi=0$, making J_y measurements useless for extracting information about ϕ. Thus, we must choose the J_x measurement. The dashed line in Fig. 1 shows that the optimal operating point is $\phi=0$ (or, more generally, $\phi=q\pi$). Near $\phi=0$, the expectation value and variance of J_x are given by

$$\langle J_x\rangle_\phi \simeq J - \frac{J(2J-1)}{2}\phi^2, \tag{5.32}$$

$$(\Delta J_x)^2_\phi \simeq J(2J-1)\phi^2, \tag{5.33}$$

where the approximations hold for $\phi \ll 1/\sqrt{J}$. The resulting optimal sensitivity,

$$\delta\phi = \frac{(\Delta J_x)_\phi}{|d\langle J_x\rangle_\phi/d\phi|} \simeq \frac{1}{\sqrt{J(2J-1)}}, \tag{5.34}$$

has the $O(J^{-1})$ sensitivity scaling found in [15].

We can relate these results to the general lower-bound analysis in Sec. III by noting that $\beta=\pi/2$ means that $\langle h\rangle = \langle Z\rangle/2=0$. This means that the dominant sums in the expansions of Eqs. (3.4) and (3.6) are those that contain only squares of h_j's. The number of terms in these sums scales as $O(n^k)$, which yields a sensitivity that scales as $O(n^{-k/2})$.

To gain further insight into the scaling behavior, we plot the scaling exponent ξ in $\delta\phi=O(n^{-\xi})$ as a function of β for J_x measurements (Fig. 3) and J_y measurements (Fig. 4), using three very large values of J. For J_y measurements we calculate ξ at the optimal operating point, $\phi=0$. For J_x measurements, the optimal operating point is a function of β, but a good compromise point, which works well over the entire range of β, is $1/\sqrt{2}J$, so we calculate the scaling exponent at this point for all values of β. An investigation of nearby operating points scaling as $1/J$ gives plots with no discernible differences for the large values of J under consideration. The main differences between J_x and J_y measurements are the following: (i) right at $\beta=\pi/2$, J_x measurements have a scaling exponent of 1, whereas J_y measurements provide no information about γ; (ii) for J_y measurements, the plot of scaling exponent has two humps, nearly symmetric about $\beta=\pi/4$ and $\beta=3\pi/4$, whereas for J_x measurements, the scaling exponent is better on the outside of the humps. The overall trend is for both measurements to have a scaling exponent of $\xi=3/2$ in the limit of large J, except at $\beta=0$, $\pi/2$, and π.

B. Decoherence

The coherent-state model suggests that our generalized quantum metrology scheme with initial product states should not display the fragility of entangled protocols in the presence of decoherence. We can investigate this possibility by considering independent dephasing of the effective qubits, described by the Lindblad equation

$$\dot{\rho} = -\frac{\Gamma}{2}(Z\rho Z - \rho), \tag{5.35}$$

where $\tau_2=\Gamma^{-1}$ is the dephasing time. Since dephasing commutes with the quadratic Hamiltonian, we can shunt its effects to the final time t, whence it maps the Pauli operators of each effective qubit in the following way:

$$X \to e^{-\Gamma t}X, \tag{5.36a}$$

$$Y \to e^{-\Gamma t}Y, \tag{5.36b}$$

$$Z \to Z. \tag{5.36c}$$

To obtain the effect of the decoherence on the expectation values and variances of the measured operators at the time of measurement, it is easiest to use the adjoint map [3], which for this simple case is identical to the map (5.36) and gives

$$\langle J_{x,y}\rangle_\Gamma = e^{-\Gamma t}\langle J_{x,y}\rangle_0, \tag{5.37}$$

$$(\Delta J_{x,y})^2_\Gamma = e^{-2\Gamma t}(\Delta J_{x,y})^2_0 + \frac{J}{2}(1-e^{-2\Gamma t}). \tag{5.38}$$

Here, a subscript Γ denotes the value with dephasing, and a subscript 0 denotes without dephasing. It is now easy to see that under this model of decoherence, for either of the measurements that we are considering, the sensitivity takes the form

$$\delta\gamma^2_\Gamma = \delta\gamma^2 + \frac{J(e^{2\Gamma t}-1)}{2\nu(d\langle J_{x,y}\rangle_0/d\gamma)^2} = \delta\gamma^2\left(1 + \frac{J(e^{2\Gamma t}-1)}{2(\Delta J_{x,y})^2_0}\right). \tag{5.39}$$

To assess the effects of decoherence, we now focus on J_y measurements, and we assume that through an adaptive feed-

back procedure, such as that sketched in Sec. V A, we are operating well within the central fringe, i.e., γt is somewhat smaller than $\pi/4J\cos\beta$. Inserting the $\phi=0$ values from Eqs. (5.21) and (5.23) into Eq. (5.39) yields a sensitivity

$$\delta\gamma_\Gamma = \frac{e^{\Gamma t}}{t\sqrt{\nu}}\frac{1}{\sqrt{2}J^{3/2}|\sin 2\beta|}. \tag{5.40}$$

If we now let $T=\nu t$ be the total time available for measurements involving ν probes, the optimal value of t, found by maximizing $e^{\Gamma t}/\sqrt{t}$ is $t=\tau_2/2$, gives a sensitivity

$$\delta\gamma_\Gamma = \sqrt{\frac{e}{T\tau_2}}\frac{1}{J^{3/2}|\sin 2\beta|}. \tag{5.41}$$

This result assumes that each probe can be processed in a time $\tau_2/2$, but within this constraint, the scaling is the same $O(J^{-3/2})$ scaling that applies in the absence of decoherence. This is to be contrasted with entangled inputs, where uncorrelated phase decoherence degrades the scaling from $O(J^{-2})$ to the $O(J^{-3/2})$ characteristic of product inputs.

These arguments hold for general symmetric k-body Hamiltonians, giving a sensitivity scaling $O(n^{-k+1/2})$ for initial product states subjected to uncorrelated phase decoherence. This is the same scaling achieved by initial optimal entangled states under this decoherence model [15]. On the other hand, the use of product states with k-body Hamiltonians for $k\geq 2$ can surpass both the standard quantum limit and the Heisenberg limit, even in the presence of phase decoherence.

VI. CONCLUSION

The possibility of using nonlinear Hamiltonians has the potential to open up a new frontier in quantum metrology. Quantum metrology has traditionally focused on linear Hamiltonians of the form $\gamma J_z=\gamma\Sigma_{j=1}^n Z_j/2$. The main technical challenge has been to improve on the standard quantum limit for determining the parameter γ, which scales as $O(n^{-1/2})$ and can be attained relatively easily using product input states and separable measurements. The goal of linear quantum metrology has been to achieve the Heisenberg limit for determining γ, which scales as $O(n^{-1})$ and requires the use of highly entangled input states. Nonlinear coupling Hamiltonians of the form J_z^k offer the possibility of further improvements in scaling. With the same highly entangled input states, nonlinear Hamiltonians can achieve a scaling $O(n^{-k})$. More importantly, they provide $O(n^{-k+1/2})$ scalings, better than the Heisenberg limit, for input product states and separable measurements. We expect that the generalized quantum metrology of nonlinear Hamiltonians will lead to new experiments—and, ultimately, to new devices—that take advantage of the enhanced scaling, which is available using the experimentally accessible tools of product-state inputs and separable measurements.

A notable feature of generalized quantum metrology is that the enhanced scalings available with product-state inputs do not rely on the entanglement produced by the nonlinear Hamiltonian. We reach this conclusion in this paper from a detailed analysis of the $k=2$ case, in the course of which we formulate an approximate coherent-state model of the time evolution, which applies during the period of enhanced sensitivity. In the model, a coherent state that makes an angle β to the z axis rotates with angular velocity $2\gamma J\cos\beta$. The increased rotation rate, larger by a factor of $2J\cos\beta$ than for $k=1$, accounts for the enhanced sensitivity. Since coherent states are product states, this indicates that entanglement plays no role in the enhanced sensitivity, and it accounts for the robustness we find in the presence of phase decoherence.

Although these conclusions emerge here from the $k=2$ analysis in this paper, it is not hard to extend the coherent-state model to arbitrary k. Given the input state (5.2), the state at time $t=\phi/\gamma$ becomes

$$|\Psi_\beta(t)\rangle = e^{-i\phi J_z^k}|\Psi_\beta\rangle = \sum_m d_m e^{-i\phi m^k}|J,m\rangle. \tag{6.1}$$

The squares of the Wigner rotation-matrix elements d_m of Eq. (5.3) are a binomial distribution, which for large J, approaches a narrow Gaussian, centered at $m=\langle J_z\rangle=J\cos\beta$, with half-width $\sqrt{2J+1}\sin\beta$. This encourages us to approximate m^k in the phases of Eq. (6.1) as $(J\cos\beta+\Delta m)^k \simeq (J\cos\beta)^k+k(J\cos\beta)^{k-1}\Delta m$, giving

$$\begin{aligned}|\Psi_\beta(t)\rangle &= e^{i\phi(k-1)(J\cos\beta)^k}\sum_m d_m e^{-i\phi k(J\cos\beta)^{k-1}m}|J,m\rangle \\ &= e^{i\phi(k-1)(J\cos\beta)^k}e^{-i\phi k(J\cos\beta)^{k-1}J_z}e^{-i\beta J_y}|J,J\rangle. \end{aligned}\tag{6.2}$$

This is an angular-momentum coherent state at angle β to the z axis, rotating about the z axis with angular velocity $\gamma k(J\cos\beta)^{k-1}$, which is the same enhanced rotation rate that we found in the very short-time analysis of Sec. IV. The approximation leading to the coherent state (6.2) thus extends to arbitrary k the uniform-fringe approximation, formulated for $k=2$ in Sec. V. The fringes have width $\pi/k(J\cos\beta)^{k-1}$, and the approximation provides a reasonable description of the first and second moments of J_x and J_y as long as $(J\cos\beta)^{k-2}\phi\sqrt{J}|\sin\beta|\ll 1$.

The enhanced rotation rate is responsible for the improved scaling, and just as for $k=2$, the coherent-state model indicates that the entanglement generated by the nonlinear Hamiltonian plays no role in the enhancement. In a separate work, to be presented elsewhere, we extend these ideas. We investigate in more detail the entanglement generated by the nonlinear Hamiltonian, quantifying it using standard entanglement measures and showing that the enhanced sensitivity with initial product states can be achieved with a vanishing amount of entanglement.

ACKNOWLEDGMENTS

This work was supported in part by Office of Naval Research Grant No. N00014-07-1-0304 and by the National Nuclear Security Administration of the U.S. Department of Energy at Los Alamos National Laboratory under Contract No. DE-AC52-06NA25396. One of the authors (E.B.) acknowledges financial support from the Catalan government Contract No. CIRIT SGR-00185, and from the Spanish MEC

through Contract Nos. FIS2005-01369 and QOIT (Consolider-Ingenio 2010), and travel Grant No. PR2007-0204. The author (E.B.) thanks the Department of Physics and Astronomy of the University of New Mexico for hospitality.

APPENDIX A: SYMMETRIC HAMILTONIAN WITHOUT SELF-INTERACTION TERMS

The symmetric k-body coupling without self-interactions is described by the Hamiltonian

$$\tilde{H} = \sum_{(a_1,\ldots,a_k)}^{n} h_{a_1}\cdots h_{a_k} = k! \sum_{a_1<a_2<\ldots<a_k}^{n} h_{a_1}\cdots h_{a_k} = \sum_{a_1,\ldots,a_k}^{n} h_{a_1}\cdots h_{a_k} - \binom{k}{2} \sum_{(a_1,\ldots,a_{k-1})} h_{a_1}\cdots h_{a_{k-2}} h_{a_{k-1}}^2 + \cdots, \tag{A1}$$

where in the second form we use the expansions of Sec. III A to relate $\tilde{H}$ to the Hamiltonian with self-interactions, plus corrections of which we give only the first. The analysis of the QCRB (1.6) relies on finding the largest and smallest eigenvalues of $\tilde{H}$. Since we are only interested in the leading-order scaling of the QCRB, Eq. (A1) shows that the analysis proceeds exactly as in the corresponding analysis for H in Sec. II, with the proviso that the results are only good to leading order in n. Thus for $\tilde{H}$, the QCRB (1.6), which can be achieved by using an appropriate initial entangled state, scales as $O(n^{-k})$.

For the case of initial product states for the probe, we proceed as in the comparable analysis of H in Sec. III A. Using the same trick of artfully switching between restricted and unrestricted sums, we can write

$$\langle\tilde{H}\rangle = \sum_{(a_1,\ldots,a_k)} \langle h_{a_1}\rangle\cdots\langle h_{a_k}\rangle = \sum_{a_1,\ldots,a_k} \langle h_{a_1}\rangle\cdots\langle h_{a_k}\rangle - \binom{k}{2} \sum_{(a_1,\ldots,a_{k-1})} \langle h_{a_1}\rangle\cdots\langle h_{a_{k-2}}\rangle\langle h_{a_{k-1}}\rangle^2 + O(n^{k-2}), \tag{A2}$$

$$\langle\tilde{H}^2\rangle = \sum_{(a_1,\ldots,a_{2k})} \langle h_{a_1}\rangle\cdots\langle h_{a_{2k}}\rangle + k^2 \sum_{(a_1,\ldots,a_{2k-1})} \langle h_{a_1}\rangle\cdots\langle h_{a_{2k-2}}\rangle\langle h_{a_{2k-1}}^2\rangle + O(n^{k-2}), \tag{A3}$$

$$\langle\tilde{H}\rangle^2 = \sum_{(a_1,\ldots,a_{2k})} \langle h_{a_1}\rangle\cdots\langle h_{a_{2k}}\rangle + k^2 \sum_{(a_1,\ldots,a_{2k-1})} \langle h_{a_1}\rangle\cdots\langle h_{a_{2k-2}}\rangle\langle h_{a_{2k-1}}\rangle^2 + O(n^{k-2}). \tag{A4}$$

The resulting variance of $\tilde{H}$,

$$(\Delta\tilde{H})^2 = k^2 \sum_{(a_1,\ldots,a_{2k-1})} \langle h_{a_1}\rangle\cdots\langle h_{a_{2k-2}}\rangle \Delta h_{a_{k-1}}^2 + O(n^{2k-2}), \tag{A5}$$

is the same, to leading order in n, as the variance (3.7) of H, so the remaining analysis of the optimal scaling and initial product states proceeds exactly as in Sec. III.

APPENDIX B: FIRST AND SECOND MOMENTS OF J

In this appendix we derive the first and second moments of the components of the angular momentum $\boldsymbol{J}$ for the Hamiltonian $H_\gamma = \gamma J_z^2$ considered in Sec. V.

Since J_z commutes with the Hamiltonian, it is a constant of the motion, and its moments are at all times those of the initial coherent state,

$$\langle J_z\rangle_\phi = J\cos\beta, \tag{B1}$$

$$\langle J_z^2\rangle_\phi = J^2\cos^2\beta + \frac{J}{2}\sin^2\beta. \tag{B2}$$

In finding the first and second moments involving the equatorial components of $\boldsymbol{J}$, it is convenient to work in terms of the angular-momentum raising and lowering operators, $J_\pm = J_x \pm iJ_y$, which act according to $J_\pm|J,m\rangle = \Gamma_m^\pm|J,m\pm1\rangle$, where $\Gamma_m^\pm = \sqrt{(J\mp m)(J\pm m+1)}$.

For the evolved state (5.4), we can write

$$\langle J_+\rangle_\phi = \sum_{m,m'=-J}^{J} d_m d_{m'} e^{i\phi(m'^2-m^2)}\Gamma_m^+\delta_{m',m+1} = \sum_{m=-J}^{J} d_m d_{m+1}\Gamma_m^+ e^{i\phi(2m+1)} = \cot(\beta/2)\sum_{m=-J}^{J}(J-m)d_m^2 e^{i\phi(2m+1)}, \tag{B3}$$

where the last line uses

$$d_{m+1} = \sqrt{\frac{J-m}{J+m+1}}\cot(\beta/2)d_m. \tag{B4}$$

Using Eq. (5.3) and a derivative of the binomial formula,

$$\sum_{m=-J}^{J}(J-m)\binom{2J}{J-m}a^{J+m}b^{J-m} = 2Jb(a+b)^{2J-1}, \tag{B5}$$

we obtain Eq. (5.9),

$$\langle J_+\rangle_\phi = \cot(\beta/2)e^{i\phi}\sum_{m=-J}^{J}(J-m)\binom{2J}{J-m} \times[e^{i\phi}\cos^2(\beta/2)]^{J+m}[e^{-i\phi}\sin^2(\beta/2)]^{J-m} = J\sin\beta(\cos\phi + i\sin\phi\cos\beta)^{2J-1}. \tag{B6}$$

The evaluation of the remaining second moments proceeds along the same lines. The correlation between J_z and J_x or J_y is conveniently expressed by

$$\frac{1}{2}\langle J_z J_+ + J_+ J_z\rangle_\phi = \sum_{m=-J}^{J} d_m d_{m+1}(m+1/2)\Gamma_m^+ e^{i\phi(2m+1)}$$
$$= (1/2 - J)\langle J_+\rangle_\phi + \cot(\beta/2) \times \sum_{m=-J}^{J} (J^2 - m^2) d_m^2 e^{i\phi(2m+1)}$$
$$= \frac{J(2J-1)}{2}\sin\beta(\cos\phi\cos\beta + i\sin\phi) \times (\cos\phi + i\sin\phi\cos\beta)^{2(J-1)}, \quad \text{(B7)}$$

where we use

$$\sum_{m=-J}^{J} (J^2 - m^2)\binom{2J}{J-m} a^{J+m} b^{J-m} = 2J(2J-1)ab(a+b)^{2(J-1)}. \quad \text{(B8)}$$

To find the second moments that involve only the equatorial components, we use

$$J_x^2 + J_y^2 = \frac{1}{2}(J_+ J_- + J_- J_+), \quad \text{(B9a)}$$

$$J_x^2 - J_y^2 = \frac{1}{2}(J_+^2 + J_-^2), \quad \text{(B9b)}$$

$$J_x J_y + J_y J_x = \frac{1}{2i}(J_+^2 - J_-^2), \quad \text{(B9c)}$$

from which we obtain

$$\langle J_{x,y}^2\rangle_\phi = \frac{1}{4}\langle J_+ J_- + J_- J_+\rangle_\phi \pm \frac{1}{2}\mathrm{Re}(\langle J_+^2\rangle_\phi), \quad \text{(B10a)}$$

$$\langle J_x J_y + J_y J_x\rangle_\phi = \mathrm{Im}(\langle J_+^2\rangle_\phi). \quad \text{(B10b)}$$

Thus, we calculate Eq. (5.10),

$$\frac{1}{2}\langle J_+ J_- + J_- J_+\rangle_\phi = \sum_{m=-J}^{J} (J + J^2 - m^2) d_m^2 = J + \frac{J(2J-1)}{2}\sin^2\beta, \quad \text{(B11)}$$

where we use Eq. (B8), and we calculate Eq. (5.11),

$$\langle J_+^2\rangle_\phi = \sum_{m=-J}^{J} d_m d_{m+2} e^{4i\phi(m+1)}\Gamma_{m+1}^+\Gamma_m^+$$
$$= \cot^2(\beta/2)\sum_{m=-J}^{J}(J-m)(J-m-1)d_m^2 e^{4i\phi(m+1)}$$
$$= \frac{J(2J-1)}{2}\sin^2\beta(\cos 2\phi + i\sin 2\phi\cos\beta)^{2(J-1)}, \quad \text{(B12)}$$

where we use

$$\sum_{m=-J}^{J}(J-m)(J-m-1)\binom{2J}{J-m} a^{J+m} b^{J-m} = 2J(2J-1)b^2(a+b)^{2(J-1)}. \quad \text{(B13)}$$

The equatorial second moments listed in Eq. (5.16) and the cross moment

$$\frac{1}{2}\langle J_x J_y + J_y J_x\rangle_\phi = \frac{1}{2}\mathrm{Im}(\langle J_+^2\rangle_\phi) = \frac{J(2J-1)}{4}\sin^2\beta R^{2(J-1)}\sin[2(J-1)\Theta], \quad \text{(B14)}$$

follow from inserting these results into Eqs. (B9).

We now make the uniform-fringe approximation of Sec. V, keeping only the fringe terms near $\phi=0$. This approximation requires that $\sqrt{J}\phi|\sin\beta| \ll 1$, but allows $J\phi\cos\beta$ to be considerably larger than 1 when $J\cot^2\beta$ is large. The resulting first and second moments,

$$\langle J_z\rangle_\phi = J\cos\beta, \quad \text{(B15a)}$$

$$\langle J_+\rangle_\phi \simeq J\sin\beta e^{2iJ\phi\cos\beta}, \quad \text{(B15b)}$$

$$\langle J_z^2\rangle_\phi = J^2\cos^2\beta + \frac{J}{2}\sin^2\beta = \frac{J}{2} + \frac{J(2J-1)}{2}\cos^2\beta, \quad \text{(B15c)}$$

$$\frac{1}{2}\langle J_z J_+ + J_+ J_z\rangle_\phi \simeq \frac{J(2J-1)}{2}\sin\beta\cos\beta e^{2iJ\phi\cos\beta}, \quad \text{(B15d)}$$

$$\langle J_x^2\rangle_\phi \simeq \frac{J}{2} + \frac{J(2J-1)}{2}\sin^2\beta\cos^2(2J\phi\cos\beta), \quad \text{(B15e)}$$

$$\langle J_y^2\rangle_\phi \simeq \frac{J}{2} + \frac{J(2J-1)}{2}\sin^2\beta\sin^2(2J\phi\cos\beta), \quad \text{(B15f)}$$

$$\frac{1}{2}\langle J_x J_y + J_y J_x\rangle_\phi \simeq \frac{J(2J-1)}{2}\sin^2\beta\sin(2J\phi\cos\beta)\cos(2J\phi\cos\beta), \quad \text{(B15g)}$$

have the unique form of an angular-momentum coherent state. They show that in the uniform-fringe approximation, the state is an angular-momentum coherent state oriented at angle β to the z axis and rotating about the z axis with angular velocity $2\gamma J\cos\beta = 2\gamma\langle J_z\rangle$.

[1] D. J. Wineland, J. J. Bollinger, W. M. Itano, and D. J. Heinzen, Phys. Rev. A **50**, 67 (1994).
[2] J. J. Bollinger, W. M. Itano, D. J. Wineland, and D. J. Heinzen, Phys. Rev. A **54**, R4649 (1996).
[3] S. F. Huelga, C. Macchiavello, T. Pellizzari, A. K. Ekert, M. B. Plenio, and J. I. Cirac, Phys. Rev. Lett. **79**, 3865 (1997).
[4] A. M. Childs, J. Preskill, and J. Renes, J. Mod. Opt. **47**, 155 (2000).
[5] J. A. Dunningham and K. Burnett, Phys. Rev. A **70**, 033601 (2004).
[6] A. Luis, Phys. Lett. A **329**, 8 (2004).
[7] M. de Burgh and S. D. Bartlett, Phys. Rev. A **72**, 042301 (2005).
[8] P. Cappellaro, J. Emerson, N. Boulant, C. Ramanathan, S. Lloyd, and D. G. Cory, Phys. Rev. Lett. **94**, 020502 (2005).
[9] J. Beltrán and A. Luis, Phys. Rev. A **72**, 045801 (2005).
[10] V. Giovannetti, S. Lloyd, and L. Maccone, Phys. Rev. Lett. **96**, 010401 (2006).
[11] S. M. Roy and S. L. Braunstein, e-print arXiv:quant-ph/0607152.
[12] S. Boixo, S. T. Flammia, C. M. Caves, and J. M. Geremia, Phys. Rev. Lett. **98**, 090401 (2007).
[13] E. Knill, G. Ortiz, and R. D. Somma, Phys. Rev. A **75**, 012328 (2007).
[14] A. Luis, Phys. Rev. A **76**, 035801 (2007).
[15] A. M. Rey, L. Jiang, and M. D. Lukin, e-print arXiv:cond-mat/0706.3376.
[16] S. Boixo and R. D. Somma, e-print arXiv:quant-ph/0708.1330.
[17] H. L. Partner, B. D. Black, and J. M. Geremia, e-print arXiv:quant-ph/0708.2730.
[18] S. Choi and B. Sundaram, e-print arXiv:cond-mat/0709.3842.
[19] S. Boixo, C. M. Caves, A. Datta, and A. Shaji, Laser Phys. **16**, 1525 (2006).
[20] G. Gilbert, M. Hamrick, and Y. S. Weinstein, e-print arXiv:quant-ph/0612156.
[21] A. Shaji and C. M. Caves, Phys. Rev. A **76**, 032111 (2007).
[22] S. L. Braunstein and C. M. Caves, Phys. Rev. Lett. **72**, 3439 (1994).
[23] S. L. Braunstein, C. M. Caves, and G. J. Milburn, Ann. Phys. **247**, 135 (1996).
[24] C. W. Helstrom, *Quantum Detection and Estimation Theory*, 1st ed., Mathematics in Science and Engineering (Academic, New York, 1976), Vol. 123.
[25] A. S. Holevo, *Probabilistic and Statistical Aspects of Quantum Theory*, 1st ed., North-Holland Series in Statistics and Probability Theory (North-Holland, Amsterdam, 1982), Vol. 1.
[26] J. M. Geremia, J. K. Stockton, A. C. Doherty, and H. Mabuchi, Phys. Rev. Lett. **91**, 250801 (2003).
[27] B. L. Higgins, D. W. Berry, S. D. Bartlett, H. M. Wiseman, and G. J. Pryde, e-print arXiv:quant-ph/0709.2996, Nature (to be published).
[28] F. Toscano, D. A. R. Dalvit, L. Davidovich, and W. H. Zurek, Phys. Rev. A **73**, 023803 (2006).
[29] W. H. Zurek, Nature (London) **412**, 712 (2001).
[30] J. J. Sakurai, *Modern Quantum Mechanics*, 2nd ed. (Addison Wesley, New York, 1994).